Available online at www.sciencedirect.com
SCIENCE DIRECT®
Journal of Solid State Chemistry 178 (2005) 702–708
JOURNAL OF SOLID STATE CHEMISTRY
www.elsevier.com/locate/jssc

The crystal structure of the monohydrate $R_2Mo_6O_{21}\cdot H_2O$ (R = Pr, Nd, Sm, and Eu): a layer structure containing disordered $[Mo_2O_7]^{2-}$ groups

Haruo Naruke*, Toshihiro Yamase

Chemical Resources Laboratory, Tokyo Institute of Technology, 4259 Nagatsuta, Midori-ku, Yokohama-shi, Kanagawa-ken 226-8503, Japan

Received 6 October 2004; received in revised form 14 December 2004; accepted 15 December 2004

Abstract

Although R_2O_3:MoO_3 = 1:6 (R = rare earth) compounds are known in the R_2O_3–MoO_3 phase diagrams since a long time, no structural characterization has been achieved because a conventional solid-state reaction yields powder samples. We obtained single crystals of $R_2Mo_6O_{21}\cdot H_2O$ (R = Pr, Nd, Sm, and Eu) by thermal decomposition of $[R_2(H_2O)_{12}Mo_8O_{27}]\cdot nH_2O$ at around 685–715 °C for 2 h, and determined their crystal structures. The simulated XRD patterns of $R_2Mo_6O_{21}\cdot H_2O$ were consistent with those of previously reported R_2O_3:MoO_3 = 1:6 compounds. All $R_2Mo_6O_{21}\cdot H_2O$ compounds crystallize isostructurally in tetragonal, $P4/ncc$ (No. 130), a = 8.9962(5), 8.9689(6), 8.9207(4), and 8.875(2) Å; c = 26.521(2), 26.519(2), 26.304(2), and 26.15(1) Å; Z = 4; R_1 = 0.026, 0.024, 0.024, and 0.021, for R = Pr, Nd, Sm, and Eu, respectively. The crystal structure of $R_2Mo_6O_{21}\cdot H_2O$ consists of two $[Mo_2O_7]^{2-}$-containing layers (A and B layers) and two interstitial $R(1)^{3+}$ and $R(2)^{3+}$ cations. Each $[Mo_2O_7]^{2-}$ group is composed of two corner-sharing $[MoO_4]$ tetrahedra. The $[Mo_2O_7]^{2-}$ in the B layer exhibits a disorder to form a pseudo-$[Mo_4O_9]$ group, in which four Mo and four O sites are half occupied. $R(1)^{3+}$ achieves 8-fold coordination by O^{2-} to form a $[R(1)O_8]$ square antiprism, while $R(2)^{3+}$ achieves 9-fold coordination by O^{2-} and H_2O to form a $[R(2)(H_2O)O_8]$ monocapped square antiprism. The disorder of the $[Mo_2O_7]^{2-}$ group in the B layer induces a large displacement of the O atoms in another $[Mo_2O_7]^{2-}$ group (in the A layer) and in the $[R(1)O_8]$ and $[R(2)(H_2O)O_8]$ polyhedra. A remarkable broadening of the photoluminescence spectrum of $Eu_2Mo_6O_{21}\cdot H_2O$ supported the large displacement of O ligands coordinating Eu(1) and Eu(2).

Keywords: Rare-earth molybdate; Lanthanide molybdate; Crystal structure; Disorder; Thermal decomposition; Polyoxomolybdate; Photoluminescence

1. Introduction

The chemistry and physics of rare-earth molybdates (REMs) with a general formula $mR_2O_3\cdot nMoO_3$ (R = rare earth; m, n = integers) was in focus for more than three decades owing to their versatile solid-state properties [1–7]. Recently, we prepared REMs by rapid thermal decompositions of a precursor compound, $[R_2(H_2O)_{12}Mo_8O_{27}]\cdot nH_2O$ [8–13]. This preparation process, a type of self flux method involving the sublimation of MoO_3, is advantageous in the research of new REMs and the growth of their single crystals, as compared to conventional solid-state reactions that usually yield samples in the powder form. To date, we have determined the structures of four compositions, of which R_2O_3:MoO_3 = 1:5 [11], 2:7 [8,10,13], and 3:10 [8] are most recent, and 1:4 for R = Nd–Tb [9,11,12] had been previously known but structurally undetermined.

The compounds with a R_2O_3:MoO_3 = 1:6 ratio, were first reported by Mokhosoev et al. [14] for R = Nd. Subsequently, Rode et al. [15] and Andryushin et al. [16] observed this composition for R = La and Sm, and R = Eu, respectively, in their phase equilibrium studies.

*Corresponding author. Fax: +81 45 924 5271.
E-mail address: hnaruke@res.titech.ac.jp (H. Naruke).

0022-4596/$ - see front matter © 2004 Published by Elsevier Inc.
doi:10.1016/j.jssc.2004.12.021

The X-ray diffraction (XRD) data of R_2O_3:$MoO_3 = 1{:}6$ including the d spacings vs. intensities were reported by Gokhman et al. [17] for R = La–Gd, and independently by Megumi et al. [18] for R = Gd. However, the diffraction patterns presented by the two groups were completely dissimilar. Recently, Yamazaki et al. [19] reinvestigated the Pr_2O_3–MoO_3 system in detail and confirmed that the XRD pattern of Pr_2O_3:$MoO_3 = 1{:}6$ was consistent with the result of Gokhman et al. Gokhman and Megumi stated that they obtained single crystals of R_2O_3:$MoO_3 = 1{:}6$, but no crystal structure has been published thereafter. Gokhman et al. [17] reported that the compound has zeolitic water (i.e., $R_2Mo_6O_{21}\cdot xH_2O$), which is removable on heating at 190 °C. This led us to anticipate a porous structure. The structure of the R_2O_3:$MoO_3 = 1{:}6$ phase thus remains undetermined.

Herein, we describe the crystal structure of R_2O_3:$MoO_3 = 1{:}6$ (R = Pr, Nd, Sm, Eu) for the first time. The compound is $R_2Mo_6O_{21}\cdot H_2O$ and it possesses highly disordered molybdate groups and a monohydrated R center.

2. Experimental

2.1. Preparation and thermal decomposition of $[R_2(H_2O)_{12}Mo_8O_{27}]\cdot nH_2O$ (R = Pr, Nd, Sm, Eu, Gd)

Polycrystalline precursor compounds $[R_2(H_2O)_{12}Mo_8O_{27}]\cdot nH_2O$ ($n = 6-9$) were prepared on the basis of our literature [9,11,12]. The precursor (0.1 g) was decomposed in air for 2 h at 685 °C for R = Pr, at 695 °C for R = Nd, at 700 °C for R = Sm, at 705 °C for R = Eu, and at 715 °C for R = Gd, and was subsequently quenched by exposure to ambient temperature to form partially fused solids. These temperatures were chosen so that they are 0–5 °C lower than melting points of the corresponding precursors. Firing at higher temperatures resulted in formation of non-crystalline glassy products. The result of the XRD measurements for the decomposed products (Fig. 1) reveals that all samples were mixtures of $R_2Mo_6O_{21}\cdot H_2O$ and MoO_3 (and $R_2Mo_4O_{15}$ for R = Pr and Sm). Platelet single crystals of $R_2Mo_6O_{21}\cdot H_2O$ formed on the surface of the product solids were carefully isolated using a needle and subjected to X-ray crystallography. The crystallization of the R = Gd phase was unsuccessful.

2.2. X-ray crystallography

Powder XRD patterns of the decomposed samples were measured at 25 °C on Rigaku RINT Ultima+/PC using graphite-monochromatized Cu$K\alpha$ (1.54184 Å) radiation. The 2θ angle was scanned from 2° to 40° at a rate of 2 ° min^{-1}.

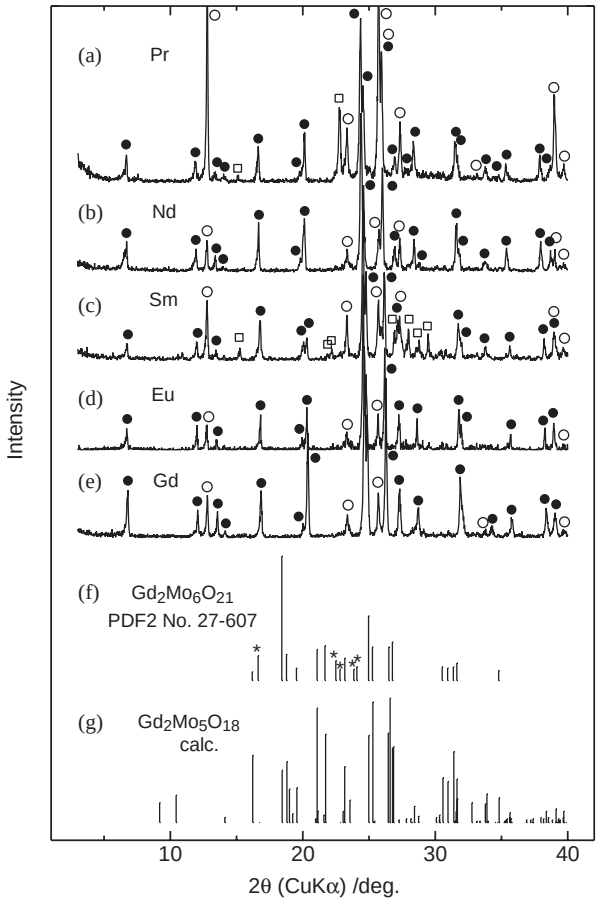

Fig. 1. XRD patterns of samples obtained by firing $[R_2(H_2O)_{12}Mo_8O_{27}]\cdot nH_2O$ at (a) 685 °C for 2 h for R = Pr, (b) at 695 °C for 2 h for R = Nd, (c) at 700 °C for 2 h for R = Sm, (d) at 705 °C for 2 h for R = Eu, and (e) at 715 °C for 2 h for Gd. (f) XRD pattern of $Gd_2Mo_6O_{21}$ (PDF2 27-607) reported by Megumi et al. [18]. (g) Simulated XRD pattern of $Gd_2Mo_5O_{18}$ [11]. Asterisked peaks in (f) are unidentified diffractions.

Single crystals of $R_2Mo_6O_{21}\cdot H_2O$ were fixed on glass fibers and mounted on a Rigaku RAXIS-RAPID imaging-plate X-ray diffractometer using graphite-monochromatized Mo$K\alpha$ radiation (0.71069 Å). Reflection intensities were collected at 25 °C. The space group $P4/ncc$ (No. 130) was determined exclusively from reflection conditions, $0\,k\,l$: $l = 2n$, $h\,k\,0$: $h + k = 2n$, $h\,h\,l$: $l = 2n$. Structures were solved by SIR92 [20] and were refined using full-matrix least-squares techniques for all the unique reflections (some reflections were removed: see the footnote of Table 1). All the atoms were refined anisotropically. Numerical absorption correction was performed using SHAPE [21] and NUMABS [22]. All calculations were carried out using the software package, CrystalStructure [23]. The complete crystallographic data and results of the refinements, refined atomic parameters, selected interatomic distances for $Pr_2Mo_6O_{21}\cdot H_2O$ are summarized in Tables 1, 2, and 3, respectively. Further details of the crystal structures for all the compounds can be obtained

Table 1
Crystallographic data and results of the structural analyses

Formula	$Pr_2Mo_6O_{21}\cdot H_2O$	$Nd_2Mo_6O_{21}\cdot H_2O$	$Sm_2Mo_6O_{21}\cdot H_2O$	$Eu_2Mo_6O_{21}\cdot H_2O$
Formula weight	1211.46	1218.12	1230.44	1233.56
Crystal size (mm^3)	$0.03\times0.04\times0.13$	$0.03\times0.09\times0.11$	$0.05\times0.05\times0.09$	$0.04\times0.07\times0.07$
Crystal system	Tetragonal	Tetragonal	Tetragonal	Tetragonal
Space group (No.)	$P4/ncc$ (No. 130)	$P4/ncc$ (No. 130)	$P4/ncc$ (No. 130)	$P4/ncc$ (No. 130)
Unit cell dimensions (Å)	$a = 8.9962(5)$	$a = 8.9689(6)$	$a = 8.9207(4)$	$a = 8.919(6)$
	$c = 26.521(2)$	$c = 26.519(2)$	$c = 26.304(2)$	$c = 26.30(2)$
Volume ($Å^3$)	2146.4(2)	2133.2(3)	2093.2(2)	2092(2)
Z	4	4	4	4
D_{calc} ($g\,cm^{-3}$)	3.749	3.793	3.904	3.916
μ (Mo$K\alpha$) (cm^{-1})	79.03	82.64	90.87	94.47
F(000)	2192	2200	2216	2224
Crystal color and habit	Pale green, plate	Pale purple, plate	Pale yellow, plate	Colorless, plate
No. of reflections				
Total	3751	11548	3680	25296
Unique (R_{int})	1577 (0.021)	1567 (0.051)	1539 (0.017)	1533 (0.061)
Used for refinement[a]	1576	1566	1524	1526
Transmission factor	0.358–0.807	0.392–0.774	0.431–0.655	0.534–0.698
No. of variables	81	81	81	81
R_w (all data)[b]	0.077	0.067	0.057	0.069
R_1[c]	0.026	0.024	0.024	0.021
w (A, B, C)[d]	5×10^{-4}, 0.4, 5×10^{-4}	2×10^{-4}, 0.3, 5×10^{-4}	1×10^{-4}, 0.5, 5×10^{-3}	5×10^{-4}, 0.3, 1×10^{-2}
Goodness of fit	0.806	0.845	0.828	0.848
$\Delta\rho_{max}$ ($e^-\,Å^{-3}$)	2.52	1.81	5.74	4.57
$\Delta\rho_{min}$	−1.13	−1.86	−2.62	−1.92

[a]Reflections having F_{obs}'s with large deviations from F_{calc}'s (with a criterion $\Delta F/\sigma F > 10$) have been removed.
[b]$R_w = \{\sum[w(F_o^2-F_c^2)^2]/\sum[w(F_o^2)^2]\}^{1/2}$.
[c]$R_1 = \sum||F_o|-|F_c||/\sum|F_o|$ for $I > 2\sigma(I)$.
[d]$w(A, B, C) = [\{AF_o^2 + B\sigma(F_o^2) + C\}/(4F_o^2)]^{-1}$.

Table 2
Atomic coordinates, equivalent isotropic displacement parameters B_{eq} ($Å^2$), site occupancies (Occ), and bond valence sums (BVS) for $Pr_2Mo_6O_{21}\cdot H_2O$

Atom	x	y	z	B_{eq}	Occ	BVS
Pr(1)	−0.2500	0.7500	0.32312(2)	1.010(7)	1.0	3.6
Pr(2)	0.2500	0.2500	0.46631(2)	1.100(7)	1.0	3.3
Mo(1)	−0.0877(1)	0.3677(1)	0.26911(4)	2.49(2)	0.5	5.6
Mo(2)	0.07172(5)	0.64697(5)	0.42700(2)	1.440(8)	1.0	6.2
O(1)	−0.0317(6)	0.6861(5)	0.3743(2)	4.6(1)	1.0	
O(2)	−0.1417(6)	0.5492(6)	0.2754(2)	5.6(2)	1.0	
O(3)	0.0957(5)	0.4575(4)	0.4322(1)	2.65(9)	1.0	
O(4)	0.2500	0.2500	0.3715(3)	2.2(1)	1.0	
O(5)	−0.2500	0.2500	0.2500	5.9(2)	1.0	
O(6)	−0.044(1)	0.288(2)	0.3330(6)	8.7(4)	0.5	
O(7)	−0.0290(6)	0.7102(5)	0.4774(2)	4.7(1)	1.0	
O(8)	0.2500	0.7500	0.4271(2)	3.4(1)	1.0	

$B_{eq} = 8/3\pi^2(U_{11}(\mathbf{aa^*})^2 + U_{22}(\mathbf{bb^*})^2 + U_{33}(\mathbf{cc^*})^2 + 2U_{12}(\mathbf{aa^*bb^*})\cos\gamma\, U_{13}(\mathbf{aa^*cc^*})\cos\beta\, U_{23}(\mathbf{bb^*cc^*})\cos\alpha)$.

from the Fachinformationszetrum Karlsruhe, 76344 Eggenstein-Leopoldshafen, Germany (fax: (49)7247-808-666; E-mail: crysdata@fiz-karlsruhe.de; URL: http://www.fiz-karlsruhe.de) on quoting the depository numbers CSD-414442 ($Pr_2Mo_6O_{21}\cdot H_2O$), CSD-414446 ($Nd_2Mo_6O_{21}\cdot H_2O$), CSD-414444 ($Sm_2Mo_6O_{21}\cdot H_2O$), and CSD-414445 ($Eu_2Mo_6O_{21}\cdot H_2O$).

2.3. Photoluminescence spectra

The decomposition product for $R = Eu$ (a mixture of $Eu_2Mo_6O_{21}\cdot H_2O$ and MoO_3) cooled to 77 K in a cryostat (Oxford CF204) was exposed to 395-nm-light (corresponding to Eu^{3+}: $^7F_0 \rightarrow {}^5L_6$ absorption) from light-emitting diodes. The resulting red emission from

Table 3
Selected interatomic distances (Å) in $Pr_2Mo_6O_{21} \cdot H_2O$

Pr(1)	—O1	×4	2.456(5)
	—O2	×4	2.412(6)
Pr(2)	—O3	×4	2.496(4)
	—O4	×1	2.516(8)
	—O7	×4	2.512(5)
Mo(1)	—O2	×1	1.711(6)
	—O2	×1	1.707(6)
	—O5	×1	1.874(1)
	—O6	×1	1.88(1)
Mo(2)	—O1	×1	1.715(5)
	—O3	×1	1.723(4)
	—O7	×1	1.711(6)
	—O8	×1	1.8524(5)

$Eu_2Mo_6O_{21} \cdot H_2O$ (MoO_3 is non-luminescent) was analyzed with a monochromator (Spex 750 M) equipped with a photomultiplier (Hamamatsu R928). The output signal was processed with a lock-in amplifier (NF LI-574), which was guided to a recorder (Riken Denshi F-45). For the purpose of comparison, the spectrum of $Eu_2Mo_5O_{18}$ single crystals at 77 K was also measured.

3. Results and discussion

3.1. Formation of the R_2O_3:MoO_3 = 1:6 phase

Figs. 1(a)–(e) show XRD patterns of samples obtained by the decomposition of $[R_2(H_2O)_{12}Mo_8O_{27}] \cdot nH_2O$ (R = Pr–Gd). The diffraction peaks for R = Pr–Eu marked with ● in Figs. 1(a)–(d) match the simulated patterns (not shown) of $R_2Mo_6O_{21} \cdot H_2O$ calculated from the single crystal data. The remaining peaks have been identified as MoO_3 (○) and $R_2Mo_4O_{15}$ (for R = Pr and Sm, (□)). Hence, the decomposition process of the precursor can be schematized as follows:

$$[R_2(H_2O)_{12}Mo_8O_{27}] \cdot nH_2O \rightarrow R_2Mo_6O_{21} \cdot H_2O + 2MoO_3 + (11+n)H_2O, \quad (1)$$

$$R_2Mo_6O_{21} \cdot H_2O \rightarrow R_2Mo_4O_{15} + 2MoO_3 + H_2O. \quad (2)$$

Attempts to prepare a single $R_2Mo_6O_{21} \cdot H_2O$ phase through control of the heating temperature and reaction time failed. Although the growth of the $Gd_2Mo_6O_{21} \cdot H_2O$ single crystal has been unsuccessful, the diffraction pattern for R = Gd (Fig. 1(e)) resembles that for other R species, suggesting the formation of an isostructural phase. All of the XRD patterns for $R_2Mo_6O_{21} \cdot H_2O$ (R = Pr–Gd) are in good agreement with those for $R_2Mo_6O_{21} \cdot xH_2O$ reported by Gokhman et al. [17] (PDF2 numbers: 32-880 for R = Pr, 32-675 for R = Nd, 32-982 for R = Sm, and 32-385 for R = Gd) and for $Pr_2Mo_6O_{21}$ by Yamazaki et al. [19], both are obtained by firing a R_2O_3:MoO_3 = 1:6 mixture. Additionally, IR spectra for $R_2Mo_6O_{21} \cdot H_2O$ (unpublished data) are also consistent with that for $Pr_2Mo_6O_{21} \cdot xH_2O$ reported by Gokhman et al. [17]. We conclude that the two preparations (thermal decomposition and solid-state reaction) result in an identical R_2O_3:MoO_3 = 1:6 phase. Gokhman et al. did not mention anything regarding the origin of the lattice water (xH_2O). The water might result due to the impurity in R_2O_3, which is considered to be hydroscopic.

Megumi et al. [18] also reported the XRD pattern of $Gd_2Mo_6O_{21}$ (PDF2 number: 27-607, Fig. 1(f)) which was obtained by firing a R_2O_3:MoO_3 = 1:6 mixture at 700 °C, annealing at 720 °C, and quenching at room temperature. The pattern is, however, different from that of $Gd_2Mo_6O_{21} \cdot H_2O$ ((●) in Fig. 1(e)) and that reported by Gokhman et al. [17]. We compared the pattern of Fig. 1(f) with several other Gd_2O_3–MoO_3 compounds. Fig. 1(g) shows a calculated pattern of $Gd_2Mo_5O_{18}$ [11], a recently discovered metastable phase not existing in the known Gd_2O_3–MoO_3 phase diagram [18]. From the 22 diffraction angles of $Gd_2Mo_6O_{21}$ reported by Megumi et al. (Fig. 1(f)), 17 are consistent with those of $Gd_2Mo_5O_{18}$ (Fig. 1(g)), and five are unidentified (asterisked peaks in Fig. 1(f)). Megumi et al. showed the molar ratio of Gd_2O_3 in their product to be 16.5–18%, which is larger than the calculated value (14.3%) of $Gd_2Mo_6O_{21}$, but close to that (16.7%) of $Gd_2Mo_5O_{18}$. These facts strongly suggest that the sample prepared by Megumi et al. was a mixture of $Gd_2Mo_5O_{18}$ (probably formed from $Gd_2Mo_6O_{21}$ by loss of MoO_3) and an unknown phase or phases. It is difficult to maintain the R_2O_3:MoO_3 = 1:6 ratio at >700 °C owing to the remarkable sublimation property of MoO_3 [19].

3.2. Structure of $R_2Mo_6O_{21} \cdot H_2O$ (R = Pr, Nd, Sm, and Eu)

All the $R_2Mo_6O_{21} \cdot H_2O$ (R = Pr–Eu) compounds crystallize isostructurally in a tetragonal lattice ($P4/ncc$). Fig. 2 shows views of the R = Pr structure, which is composed of two types of $[Mo_2O_7]^{2-}$-containing layers (A and B layers) linked by Pr(1) and Pr(2) atoms through the O–Pr–O bonding. These layers parallel to the $a-b$ plane are stacked in the sequence of $\cdots(ABA)(ABA)\cdots$. Pr(1) is positioned between the A and B layers, while Pr(2) is positioned between two A layers. The A and B layers both comprise isolated $[Mo_2O_7]^{2-}$ groups formed by corner-sharing $[MoO_4]$ tetrahedra, where the bridgings O(5) and O(8) lie on the crystallographic $\bar{4}$ (S_4) axis. In the A layer, the $[Mo_2O_7]^{2-}$ group possesses 2 (C_2) symmetry with an almost linear (179.9(3)°) Mo(2)–O(8)–Mo(2)′ angle (Fig. 3(a)). In the B layer, the $[Mo_2O_7]^{2-}$ group exhibits

a disorder such that each of the four [Mo(1), Mo(1)′, Mo(1)″, and Mo(1)‴] and the four [O(6), O(6)′, O(6)″, and O(6)‴] equivalent sites are half occupied (i.e., site occupancy of 0.5), and thereby a pseudo-$[Mo_4O_9]$ group appears with a 222 (D_2) symmetry (Fig. 3(b)). Under the condition of full occupancy for Mo(1) and O(6), the Mo(1)⋯Mo(1)′ (or Mo(1)″⋯Mo(1)‴) separation (1.162(2) Å) is extremely short and the least-squares refinement diverged. Due to this disorder, four dispositions of the [MoO4]–[MoO4] tetrahedra in the $[Mo_2O_7]^{2-}$ group exist—Mo(1)–Mo(1)″, Mo(1)–Mo(1)‴, Mo(1)′–Mo(1)″, and Mo(1)′–Mo(1)‴, which exhibit two different Mo(1,1′)–O(5)–Mo(1″,1‴) angles—148.61(5) and 162.58(5)° (Fig. 3(b) and Table 2). It is noted that a remarkable flattering and/or elongation of thermal ellipsoids with relatively large B_{eq} values (5.6(2)–8.7(4) Å^2) is observed for O(2), O(5), and O(6) (Fig. 3(b), Table 2). These unusual distortions of the ellipsoids suggest that atomic positions in one [MoO4] moiety are slightly displaced depending on the two alternative positions of another [MoO4] moiety in the same $[Mo_2O_7]^{2-}$ group. Furthermore, the disorder in

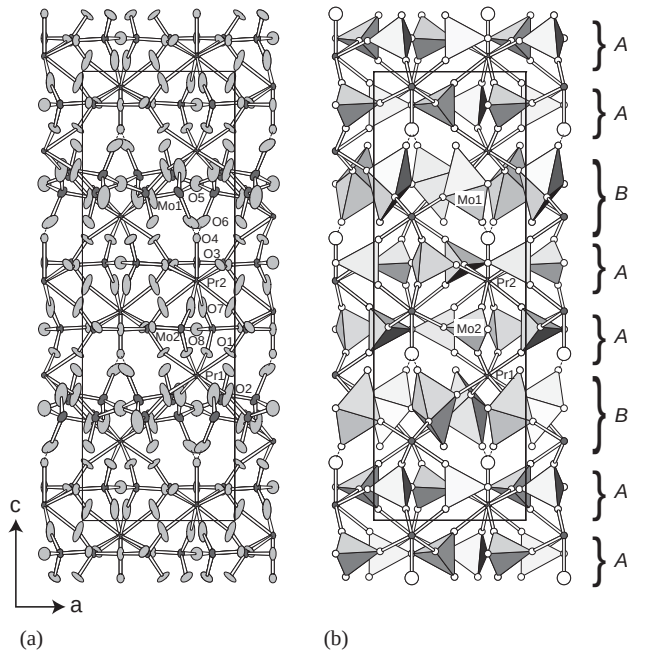

Fig. 2. Structure of $Pr_2Mo_6O_{21}\cdot H_2O$ viewed along the [100] direction represented by (a) ellipsoidal and (b) [MoO_4]-polyhedral models. Two molybdate layers are denoted by *A* and *B*. The O(4)⋯O(6) hydrogen-bonds are drawn with broken lines. Parentheses for atom labeling are omitted for clarity.

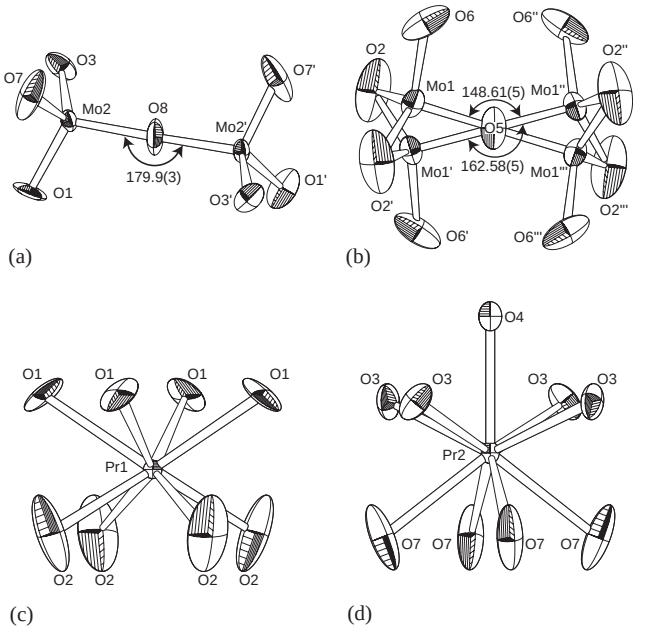

Fig. 3. Views of (a) the $[Mo_2O_7]^{2-}$ group in the *A* layer, (b) the $[Mo_2O_7]^{2-}$ (pseudo-$[Mo_2O_9]$) group in the *B* layer, (c) [Pr(1)O_8], and (d) [Pr(2)(H_2O)O_8] polyhedra. Parentheses for atom labeling are omitted for clarity.

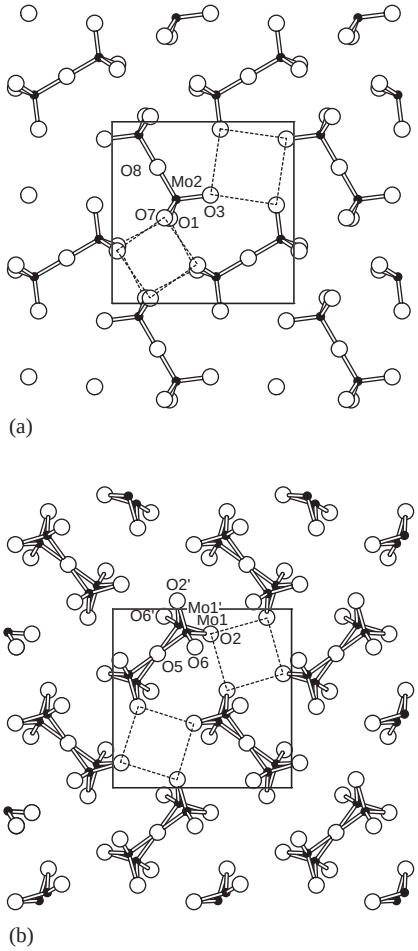

Fig. 4. Perpendicular views of the (a) *A* layer and (b) *B* layer. The square-forming O atoms of O(1), O(2), O(3), O(7) and their symmetry-related atoms coordinating the Pr(1) and Pr(2) centers are interconnected with broken lines. Parentheses for atom labeling are omitted for clarity.

the B layer gives rise to atomic displacements of the $[Mo_2O_7]^{2-}$ group in the A layer through the O–Pr–O linkage: the thermal ellipsoids for O(1), O(7), and O(8) are also flattered and/or elongated (Fig. 3(a)).

As shown in Fig. 4, the two $[Mo_2O_7]^{2-}$ groups are similarly arranged in the A and B layers: they are symmetry related by the crystallographic 4 (C_4) axis parallel to the [001] direction. The O(1), O(2), O(3), and O(7) atoms and their equivalent positions define squares (denoted with (----) in Fig. 4) that coordinate the Pr(1) and P(2) atoms. Figs. 3(c) and (d) represent coordination environments around the two Pr centers, both of which are positioned on the 4 axes. Pr(1) is square antiprismatically 8-coordinated by the square-forming four O(1) and four O(2) atoms, and Pr(2) is monocapped square antiprismatically 9-coordinated by the square-forming four O(3) and four O(7), and O(4) which caps the O(3) square. The capping O(4) atom, with a bond valence sum (BVS) [24] of 0.35, is an aqua-ligand exhibiting covalent bonding only with Pr(1) and hydrogen bonding with neighboring O(6) atoms with a distance of 2.86(1) Å ((----) in Figs. 2(a) and (b)). A similar $[R(H_2O)O_8]$ polyhedron has been observed for yttrium oxalate compounds [25,26]. The symmetry of both $[Pr(1)O_8]$ and $[Pr(2)(H_2O)O_8]$ polyhedra is well approximated to $4mm(C_{4v})$, however, the actual symmetry should be lowered by the displacements of the O(1), O(2), and O(7) ligands.

Similar to the $R = Pr$ compound, all $R = Nd$–Eu analogs showed an identical disorder of the $[Mo_2O_7]^{2-}$ group in B layer and similar distorted ellipsoids for the O(1), O(2), and O(5–8) atoms. Since spectroscopic properties of R^{3+} are sensitive to the O ligand environment, we also studied the photoluminescence of $Eu_2Mo_6O_{21}\cdot H_2O$. Fig. 5 shows photoluminescence spectra of $Eu_2Mo_6O_{21}\cdot H_2O$ and $Eu_2Mo_5O_{18}$ both of which measured at 77 K under an identical resolution condition. They exhibit red luminescence assignable to the $^5D_0 \rightarrow {}^7F_J$ ($J = 0-4$) transitions characteristic of Eu^{3+}. $Eu_2Mo_5O_{18}$ has a rigid non-disordered structure containing a crystallographically single Eu^{3+} site [11]. As shown in Fig. 5, $Eu_2Mo_6O_{21}\cdot H_2O$ displays much broad spectrum compared with $Eu_2Mo_5O_{18}$. Especially, a half line width ($\sim 25\,cm^{-1}$) of $^5D_0 \rightarrow {}^7F_0$ for $Eu_2Mo_6O_{21}\cdot H_2O$ is four times larger than that ($\sim 6\,cm^{-1}$) for $Eu_2Mo_5O_{18}$ (Fig. 5 inset). It should be noted that $^5D_0 \leftrightarrow {}^7F_0$ band does not split in any coordination field and the energy of which slightly depends on the Eu^{3+} environment. The spectrum of $Eu_2Mo_6O_{21}\cdot H_2O$ is obviously more broadened than expected by the presence of two different Eu^{3+} sites (Eu(1) and Eu(2)). The line broadening for $Eu_2Mo_6O_{21}\cdot H_2O$ is attributable to the wide distribution of the Eu^{3+} environment caused by the large displacement of the O ligands around Eu^{3+}.

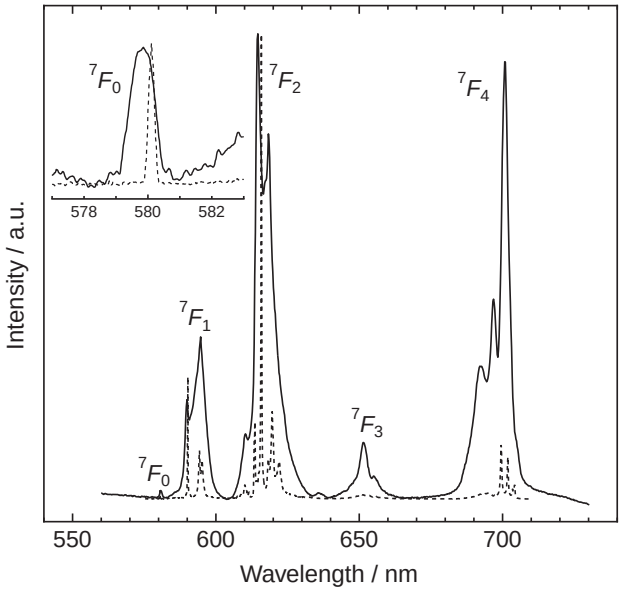

Fig. 5. Photoluminescence spectra of $Eu_2Mo_6O_{21}\cdot H_2O$ (—) and $Eu_2Mo_5O_{18}$ (----) at 77 K under excitation with 395-nm-light corresponding to the Eu^{3+}: $^7F_0 \rightarrow {}^5L_6$ absorption. Bands are assigned to the $^5D_0 \rightarrow {}^7F_J$ ($J = 0-4$) transitions. Inset: magnified $^5D_0 \rightarrow {}^7F_0$ bands.

The disorder for the $[Mo(1)_2O_7]^{2-}$ group and the large displacement of O(1, 2, 7) atoms caused apparent long Mo(1)–O and short Pr(1, 2)–O distances (Table 2) compared to normal values. Anomalous calculated BVSs [24,27] for Mo(1) (5.6), Pr(1) (3.6), and Pr(2) (3.3) (Table 2) are due to the over- and underestimations of the Pr(1, 2)–O and Mo(1)–O distances, respectively. Distances of Mo(1)–O and R(1, 2)–O for other $R = Nd$, Sm, and Eu analogs showed similar tendencies.

In conclusion, we shall briefly discuss the dehydration of $Pr_2Mo_6O_{21}\cdot xH_2O$ at 190 °C as reported by Gokhman et al. [17]. They observed that IR absorption bands due to water molecules vanished on heating. The aqua-ligand (O(4)) covalently bonded to R(2) is unlikely to be eliminated at such a low temperature. In fact, our IR measurement (unpublished data) revealed that $Pr_2Mo_6O_{21}\cdot H_2O$ is stable up to 400 °C and is dehydrated between 450 and 500 °C to be decomposed to $Pr_2Mo_4O_{15}$ via Eq. (2). Dehydration at low temperatures would be possible if $R_2Mo_6O_{21}\cdot H_2O$ possesses large pores accommodating lattice water molecules. It is notable that the disorder of the $[Mo_2O_7]^{2-}$ groups in the B layer should create O(6) vacancies. However, the capacity (two O^{2-} per a $[Mo_2O_7]^{2-}$ group) of these vacant spaces is small and is distributed randomly in the lattice that would not form an open channel. Consequently, no absorptive effect is expected for these vacancies. We observed only a small specific surface area (0.4–0.6 $m^2\,g^{-1}$) for $Pr_2Mo_6O_{21}\cdot H_2O$ by the nitrogen absorption method. Thus, the dehydration behavior

observed by Gokhman et al. cannot be explained by the crystal structure of $R_2Mo_6O_{21} \cdot H_2O$.

4. Conclusion

In this work, we determined the crystal structure of the R_2O_3:$MoO_3 = 1{:}6$ (R = Pr–Eu) phase ($R_2Mo_6O_{21} \cdot H_2O$) for the first time and showed the R = Gd analog to be isostructural. The structural data successfully explained the previous powder diffraction data of $R_2Mo_6O_{21} \cdot xH_2O$ (PDF2 numbers: 32-880 for R = Pr, 32-675 for R = Nd, 32-982 for R = Sm, and 32-385 for R = Gd) reported by Gokhman et al. The diffraction data of $Gd_2Mo_6O_{21}$ (PDF2 number: 27-607) reported by Megumi et al. were suggested to be a mixture of $Gd_2Mo_5O_{18}$ and an unknown phase or phases. $R_2Mo_6O_{21} \cdot H_2O$ is a layer compound composed of two $[Mo_2O_7]^{2-}$, one $[RO_8]$, and one $[R(H_2O)O_8]$ groups. One of the two $[Mo_2O_7]^{2-}$ groups exhibits a disorder that induces a large positional shift of the O atoms in another $[Mo_2O_7]^{2-}$ group, and $[RO_8]$ and $[R(H_2O)O_8]$ polyhedra. The resulting wide distribution of the ligand field of R^{3+} was demonstrated by the significant broadening of photoluminescnece spectrum for $Eu_2Mo_6O_{21} \cdot H_2O$. The crystal structure of $R_2Mo_6O_{21} \cdot H_2O$ cannot explain the low-temperature (190 °C) dehydration reported by Gokhman et al.

Acknowledgments

The authors wish to thank Professor Y. Morikawa and Dr. T. Mori at their institute for providing measurements of the specific surface area. Furthermore, they wish to thank Professor T. Yamazaki and Professor K. Terayama at the Toyama University for providing detailed XRD data and the preparation conditions for $Pr_2Mo_6O_{21}$ published in Ref. [19].

References

[1] K. Aizu, A. Kumada, H. Yumoto, S. Ashida, J. Phys. Soc. Japan 27 (1969) 511.
[2] H.J. Borchardt, P.E. Bierstedt, Appl. Phys. Lett. 8 (1966) 50–52.
[3] G. Blasse, A. Bril, J. Chem. Phys. 45 (1966) 2350–2355.
[4] J. Huang, J. Lories, P. Porcher, J. Solid State Chem. 43 (1982) 87–96.
[5] M. Ouwerkerk, F. Kellendonk, G. Blasse, J. Chem. Soc., Faraday Trans. 2 78 (1982) 603–611.
[6] P. Lacorre, F. Goutenoire, O. Bohnke, R. Retoux, Y. Laligant, Nature 404 (2000) 856–858.
[7] L. Sebastian, S. Sumithra, J. Manjanna, A.M. Umarji, J. Gopalakrishnan, Mater. Sci. Eng. B 103 (2003) 289–296.
[8] H. Naruke, T. Yamase, J. Solid. State Chem. 161 (2001) 85–92.
[9] H. Naruke, T. Yamase, Acta. Crystallogr. E 57 (2001) i106–i108.
[10] H. Naruke, T. Yamase, Acta Crystallogr. E 58 (2002) i62–i64.
[11] H. Naruke, T. Yamase, Inorg. Chem. 41 (2002) 6514–6520.
[12] H. Naruke, T. Yamase, J. Solid State Chem. 173 (2003) 407–417.
[13] H. Naruke, T. Yamase, J. Ceram. Soc. Japan Suppl. 112 (2004) S67–S72.
[14] M.V. Mokhosoev, E.I. Get'man, Inorg. Mater. 5 (1967) 772–776.
[15] E.Y. Rode, G.V. Lysanova, L.Z. Gokhman, Inorg. Mater. 7 (1971) 1875–1877.
[16] I. Andryushin, R.A. Belyaev, A.I. Belyakov, V.V. Bondraenko, V.P. Vyskubov, S.S. Kiparisov, V.G. Kozlov, V.A. Lazarevskii, Inorg. Mater. 12 (1976) 739–741.
[17] L.Z. Gokhman, G.V. Lysanova, D.A. Dulin, A.V. Pashkova, Russ. J. Inorg. Chem. 19 (1974) 1106–1108.
[18] K. Megumi, H. Yumoto, S. Ashida, S. Akiyama, Y. Furuhata, Mater. Res. Bull. 9 (1974) 391–400.
[19] T. Yamazaki, T. Shimazaki, T. Hashizume, K. Terayama, M. Yoshimura, J. Mater. Sci. Lett. 21 (2002) 29–31.
[20] Altomare, M.C. Burla, M. Camalli, M. Cascarano, C. Giacovazzo, A. Guagliardi, G. Polidori, J. Appl. Crystallogr. 27 (1994) 435.
[21] T. Higashi, SHAPE—Program to Obtain Crystal Shape Using CCD Camera, Rigaku Corporation, Tokyo, Japan, 1999.
[22] T. Higashi, NUMABS—Numerical Absorption Correction, Rigaku Corporation, Tokyo, Japan, 1999.
[23] Rigaku Corporation and Rigaku/MSC, Crystal Structure Ver. 3.6.0, Tokyo, Japan.
[24] D. Brown, in: M. Keeffe, A. Navrotsky (Eds.), Structure and Bonding in Crystals, vol. II, Academic Press, New York, 1980, pp. 1–30.
[25] T.R.R. Mcdonald, J.M. Spink, Acta Crystallogr. 23 (1967) 944–949.
[26] T. Bataille, D. Louër, Acta Crystallogr. C 55 (1999) 1760–1762.
[27] D. Brown, D. Altermatt, Acta Crystallogr. B 41 (1985) 244–247.